

SecONN: An Optical Neural Network Framework with Concurrent Detection of Thermal Fault Injection Attacks

Kota Nishida
Osaka University
Japan
nishida.kota@ist.osaka-u.ac.jp

Yoshihiro Midoh
Osaka University
Japan
midoh@ist.osaka-u.ac.jp

Noriyuki Miura
Osaka University
Japan
nmiura@ist.osaka-u.ac.jp

Satoshi Kawakami
Kyushu University
Japan
kawakami@ed.kyushu-u.ac.jp

Jun Shiomi
Osaka University
Japan
shiomi-jun.ist@osaka-u.ac.jp

Abstract—Silicon Photonics-based AI Accelerators (SPAAs) have been considered as promising AI accelerators achieving high energy efficiency and low latency. While many researchers focus on improving SPAAs' energy efficiency and latency, their physical security has not been sufficiently studied. This paper first proposes a threat of thermal fault injection attacks on SPAAs based on Vector-Matrix Multipliers (VMMs) utilizing Mach-Zhender Interferometers. This paper then proposes SecONN, an optical neural network framework that is capable of not only inferences but also concurrent detection of the attacks. In addition, this paper introduces a concept of Wavelength Division Perturbation (WDP) where wavelength dependent VMM results are utilized to increase detection accuracy. Simulation results show that the proposed method achieves 88.7% attack-caused average misprediction recall.

Index Terms—Silicon Photonics-based AI Accelerator (SPAA), Optical Neural Network (ONN), Thermal Fault Injection Attack

I. INTRODUCTION

Artificial Intelligence (AI)-based applications play an important role in the rapid development of our super smart society. Downscaling of CMOS transistors have continuously met ever-increasing demands for computing efficiency in our society. However, the improvement of CMOS circuit latency has been saturated since the parasitic delay becomes dominant in advanced process technologies [1]. Optical circuits have been emerged as a promising approach for resolving the latency issue of CMOS circuits. Traditionally, optical communication technologies have been utilized for long-distance efficient communication. Recent advancement in silicon photonics has enabled ever-shorter optical network-on-chip applications [2]. Recently, optical computing by silicon photonics has been extensively studied to boost up the computational efficiency. Motivated by the rapid AI development, various types of Optical Neural Networks (ONNs) have been widely studied.

This paper proposes *SecONN*, an optical neural network framework that can perform not only inference operations but also concurrent detection of thermal fault injection attacks. Recently, many start-up companies such as Lightmatter [3], Luminous and LightOn have released commercial photonics-based AI accelerators, which implies that consumers can employ

Silicon Photonics-based AI Accelerators (SPAAs) everywhere in the near future. This enables optics-based edge computing where optical computing devices are employed into midrange edge servers along with mobile devices in order to meet the ever-increasing demand for AI performance as pointed in [4]. The problem in such environments is attackers can also access SPAAs for malicious purposes. For example, Deep Neural Networks (DNNs) are widely used in mission-critical and security-sensitive systems such as autonomous driving systems. Attackers can disrupt the systems by simply injecting a tiny fault that causes the DNN to misclassify the input data as random wrong categories [5], which leads to serious accidents in the mission-critical systems. Another problem is that optical circuit elements are several orders of magnitude larger than CMOS ones. This motivates attackers to access SPAAs for malicious purposes. However, physical security of SPAAs has not been studied sufficiently yet. This paper thus firstly points out a threat of thermal fault injection attacks on SPAAs which causes misprediction of SPAAs. To tackle this issue, a concurrent attack detection technique is proposed. The contribution of this paper is summarized as follows:

- 1) This paper introduces a threat of thermal fault injection attacks on SPAAs. The measurement result shows only a single point thermal attack can fully tamper with the cross/bar state of a Mach-Zhender Interferometer (MZI), a core optical element of SPAAs. This indicates SPAAs may mispredict due to the attack. To the best of our knowledge, this is the first paper showing measurement results of thermal fault injection attacks.
- 2) This paper proposes *SecONN* featuring a concurrent monitoring technique of thermal fault injection attacks without accuracy degradation. A checksum added in the output layer monitors abnormal phase shifts caused by thermal fault injection attacks without any hardware overhead in optical circuits. In addition, this paper introduces a concept of Wavelength Division Perturbation (WDP) where wavelength-dependent Vector Matrix Multiplication (VMM) results are utilized for detection. This

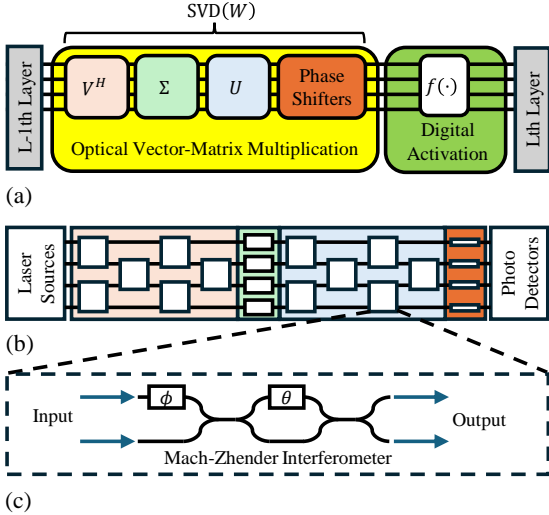


Fig. 1: (a) Overview of SPAA architecture using MZI-VMM. (b) MZI-VMM structure. (c) MZI structure.

technique amplifies the effect of abnormal phase shifts in VMMs, thereby increasing detection accuracy without degrading ONNs' latency.

- 3) A simulation environment of thermal fault injection is developed. Simulation results show *SecONN* achieves 88.7% attack-caused average misprediction recall.

The rest of this paper is organized as follows. Section II presents motivational examples and related works. In Sect. III, *SecONN* is proposed. In Sect. IV, evaluation results of *SecONN* are presented. Section V concludes this paper.

II. MOTIVATIONAL EXAMPLE AND RELATED WORK

A. Preliminaries: Optical Neural Networks

Figure 1a shows an overview of MZI-based SPAA architectures [6]. It consists of an optical VMM part and a digital activation part which correspond to linear transformations and non-linear transformations, respectively. The digital activation part is processed by a CMOS coprocessor. Fully Connected (FC) layers of neural networks can be represented as VMMs where the weight values of FC layers are set as matrix elements. The matrix is denoted as W in this paper. The optical VMM part obtains the VMM result at the L 's layer:

$$y^L = Wx^L, \quad (1)$$

where x^L and y^L are complex amplitudes of input optical signals and output optical signals, respectively. W is the multiplied matrix whose value is modulated via multiple electrical terminals. The VMM part can be decomposed as U , Σ , V^H and phase shift by the Singular Value Decomposition (SVD). Here, U and V^H are unitary matrices. Σ is a diagonal matrix.

For the VMM part, this paper utilizes an MZI-array Vector-Matrix Multiplier (MZI-VMM) as a representative of SPAA. Figure 1b shows an MZI-VMM structure. The two unitary matrices (U and V^H) are constructed by cascading MZI

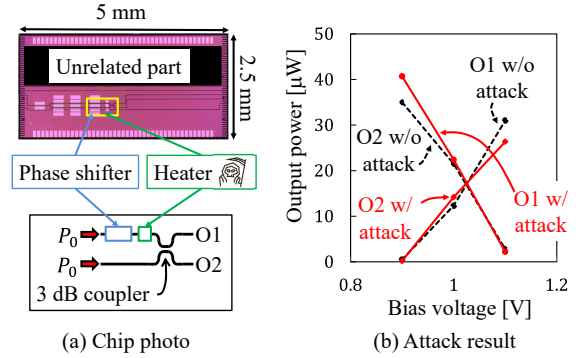


Fig. 2: Measurement result of a thermal fault injection attack.

arrays. The Clements mesh [7] is employed for constructing U and V^H . The diagonal matrix (Σ) consists of attenuators or amplifiers. The optical circuits corresponding to U and V^H are composed of multiple MZIs (white squares in Fig. 1b). MZI consists of two phase shifters and two 3 dB couplers as shown in Fig. 1c. An MZI realizes arbitrary 2×2 unitary matrix multiplication by tuning ϕ and θ . By individually tuning ϕ s and θ s of MZIs in an MZI-VMM, arbitrary VMM can be achieved.

B. Motivational Example: Thermal Fault Injection Attack

This section shows the actual measurement result of thermal fault injection attacks and their impact on ONNs as a motivational example. Figure 2a shows a photograph of a silicon photonic chip employing a digital switch. Its equivalent circuit is shown at the bottom of Fig. 2a. Two coherent light signals with the same power (P_0) are fed into two input ports, respectively. A phase shifter consisting of a PIN injection diode is on a waveguide. The phase-modulated lights are coupled at the 3 dB coupler and then fed into output ports "O1" and "O2." By tuning "Phase shifter," the "O1" and the "O2" signals can be fully switched. Figure 2b shows the measurement results where the horizontal axis and the vertical axis are the bias voltage of the PIN diode and the output light power, respectively. The black broken lines are the tuning result of "Phase shifter." This shows that the output ports "O1" and "O2" are fully switched. In typical optical circuits, near the 3 dB coupler, a thermal heater is mounted for finely tuning the phase offset based on the thermo-optic effect. We assume that the attacker can access the heater to maliciously modulate the phase. The red solid lines of Fig. 2b shows fault injection results where the bar/cross state of the switch is fully inverted. As shown in Fig. 1, SPAA consists of MZIs with phase shifters and couplers. This indicates that attackers can tamper with the entire matrix elements by accessing heaters in SPAA. Even without directly accessing heaters, attackers can locally heat any waveguides by Thermal Laser Stimulation (TLS) [8]. Optical beam can locally heat semiconductor devices, thereby resulting in the same tampering result. This means attackers can inject phase shift into any waveguide points.

To evaluate the tamper resistance of ONNs, this paper builds up the ONN simulator considering the local thermal fault injection attack as shown in Fig. 3. Although the detailed

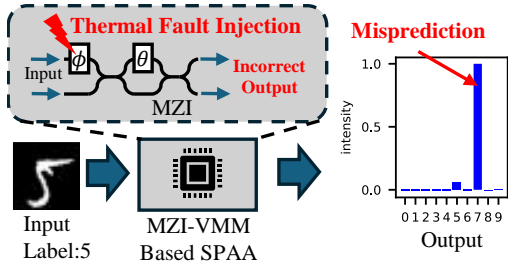


Fig. 3: Thermal fault injection attack on SPAA.

structure of the simulator and the ONN is written in Sect. III, this section briefly explains the impact of the thermal fault injection attack. We assume that the attacker can inject a π -radian phase offset to an arbitrary single phase shifter of an SPAA with a well-trained model (97.8% accuracy without attacks) targeting the MNIST handwritten digit dataset [9]. Without attacks, the SPAA can correctly classify an input image with a label “5.” If the attacker can somehow find a weak point, a single thermal fault injection attack can tamper with the intensity of the output nodes as shown in Fig. 3. The output label with the maximum intensity becomes “7.” The ONN thus mispredicts the input image as “7.” If attackers randomly inject single faults to the SPAA, the average accuracy drops to 93.8%. In the worst case, the accuracy drops to 2.5%.

Reference [10] considers a similar but different situation where temperature is uniformly increased throughout the chip. This can be monitored by just placing a temperature sensor near an SPAA macro. However, the thermal fault injection attacks only locally heat specific points in SPAA macros, which makes it hard to detect the attack by a temperature sensor. To tackle this stealthiness issue, this paper proposes an ONN framework with concurrent detection of thermal fault injection attacks.

C. Related Work

Fault Attacks (FAs) are serious physical attacks where intentional faults are induced in cryptographic circuits and secret key information is revealed by analyzing the erroneous output and the correct output. The concept of FAs was firstly proposed by [11]. In order to induce intentional faults, for example, attackers use abnormal clock signals [12] and voltage fluctuation [13]. A laser fault injection attack has also emerged as a powerful FA method [14] where faults can be accurately injected by laser beams to flip-flops at arbitral specific positions in chips.

Although FAs were originally proposed to attack cryptographic circuits, it is now recognized that attackers can use FAs for inducing misprediction of DNN-based applications. DNNs are widely used in mission-critical and security-sensitive systems such as autonomous driving systems. If attackers can induce misprediction of DNNs in such systems, these attacks can cause serious damage to the systems. To induce intentional faults, attackers tamper with parameters stored in memories [5] or with activation results [15]. Basic countermeasures are to test the circuits [16], to employ fault-tolerant redundant data formats [17] and to employ sensors of FAs [18]. The

problem is ONNs are an analog optical computation paradigm. Conventional testing and fault-tolerant approaches are for digital CMOS circuits. It thus can not be directly utilized for analog SPAAs. Redundant analog formats significantly increase the hardware cost. Another problem is it is hard to directly use conventional CMOS-based FA sensor techniques for non-CMOS optics-based elements. This paper proposes a runtime detection technique of thermal fault injection attacks on ONNs.

The physical security of optical circuits has not been fully studied so far. References [19], [20] point out optical circuits have the potential to achieve tamper-resistant logical operations against side-channel attacks which reveal secret information by measuring optical signals inside optical circuits. Although their techniques work well for side-channel attacks, they do not target how to protect against invasive FAs targeted in this paper. Reference [21] points out that adversarial attacks on SPAAs, where small noises are injected into input images to induce misprediction, are theoretically possible. However, they do not point out how to protect SPAAs against adversarial attacks. Reference [10] points out the SPAAs’ vulnerability to thermal cross talk. The malicious optical circuits can increase their own temperature. Thus, the temperature of the victim optical circuits near the malicious one is increased by the thermal cross talk, which induces erroneous outputs. Reference [10] proposes a simple attack detection method. Test signals are fed into the ONNs, and the output signals are compared with the expected outputs. If we simply utilize this technique to detect thermal fault injection attacks, this paper points out that it will degrade SPAAs’ potential performance. Without the degradation, this paper targets the detection method of thermal fault injection attacks which are more aggressive invasive attacks on SPAAs.

III. SECONN FRAMEWORK

A. Threat Model

Assuming that attackers can access SPAAs, this paper targets the threat model where attackers can locally inject single phase shift errors into arbitral phase shifters in SPAAs. Specifically, the attacker injects a phase error into one of phase shifters in an SPAA (θ_s and ϕ_s in Fig. 1c) during the inference operation of each input data. Considering the situation for mission-critical systems, attackers attempt to cause DNNs to misclassify the input data as random wrong categories for inducing serious damage to the systems.

B. Overview

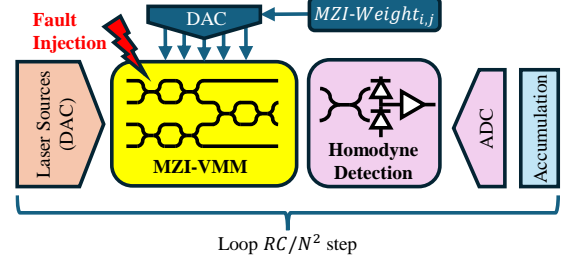
This paper proposes *SecONN*, a neural network framework that is capable of concurrently detecting thermal fault injection attacks. Figure 4 shows the overview of the framework. This framework features the following three flows: (1) Training, (2) Weight conversion and (3) Inference. “(1) Training” features a training flow considering the concurrent detection technique inspired by the balanced output partition technique [22]. This technique is presented in Sect. III-D. In “(2) Weight conversion,” weight values in ONNs are converted to phase shift values of MZIs (ϕ_s and θ_s in Fig. 1c). “(3) Inference” includes inference frameworks including the balanced output partition

technique and a fault injection simulator. This paper proposes a concept of *Wavelength Division Perturbation (WDP)* where abnormal phase shifts are amplified by feeding multiple lights with different wavelengths. *SecONN* also features a simulation environment which is firstly presented in Sect. III-C.

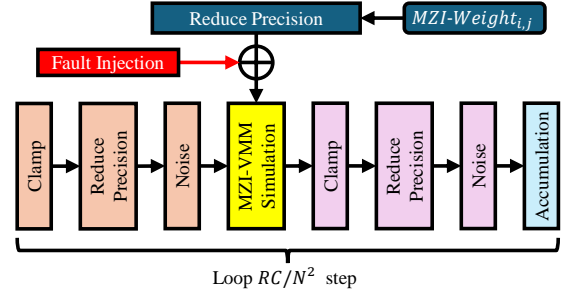
C. Simulation Framework

The proposed framework converts weight values of target neural network into phase shift values of MZIs (ϕ s and θ s in Fig. 1c). The simulator then obtains optical characteristics (amplitudes and phases) of output lights in each layer considering thermal fault injection attacks.

This paper extends *AnalogVNN* [23], a simulation framework for optical neural networks. Figure 5 illustrates the *AnalogVNN* framework. *AnalogVNN* comprises a Digital-Analog Conversion (DAC) layer, a linear Operation (“Conv/FC”) layer, and an Analog-Digital Conversion (ADC) layer. DAC and ADC layers consist of normalization, precision reduction, and noise addition. The latter two layers quantize the inputs and add the Gaussian noise to them, respectively. In “Conv/FC,” VMM for a target layer (L 'th layer in this case) is performed based on preprocessed analog inputs and weight values. *AnalogVNN* itself only numerically calculates VMM expressed in Eq. (1) during the linear operation. *AnalogVNN* does not consider thermal fault injections. In order to evaluate thermal fault injections, firstly W in Eq. (1) needs to be decomposed to a set of phase shift values in each MZI (ϕ s and θ s in Fig. 1c).



(a) The target SPAA architecture.



(b) The layer design of Fig. 6a.

Fig. 6: The target SPAA and its layer design.

Generally, a small MZI-VMM needs to be reutilized multiple times for obtaining the entire VMM result due to the hardware resource limitation. This is not also considered in *AnalogVNN* but needs to be considered since fault injection points in the MZI-VMM need to be set for evaluating the tamper resistance.

To evaluate the impact of thermal fault injection attacks on devices, the decomposition flow is implemented to *AnalogVNN*. The flow is as follows: (1) Model training without MZI-VMM simulation (numerical optimization of W in Eq. (1) only), (2) Conversion of the weights for the MZI-VMM (decomposition to ϕ s and θ s in Fig. 1c), and (3) Inference operation with the MZI-VMM simulator. In (2) and (3), this paper targets the optical VMM architecture illustrated in Fig. 6a. This architecture has a set of MZI-VMM of matrix size N and homodyne detectors. It numerically calculates MZI-VMM results RC/N^2 times, where R and C are the numbers of rows and columns of the matrix W in Eq. (1), respectively. The multiplication results are accumulated digitally to obtain the $R \times C$ -size VMM result. The input laser and the output signals of the ADC are quantized with A -bit precision. Similarly, the signals to set weights are quantized. Figure 6b shows the layer design. We replace the linear layer in Fig. 5 with the in-house MZI-VMM simulator [24]. This simulator decomposes weight values to ϕ s and θ s in Fig. 1c by the decomposition flow of [7].

D. ONN for Concurrent Detection

This paper utilizes balanced output partitions presented in [22] for concurrently detecting thermal fault injection attacks. It is originally designed to concurrently detect hardware faults such as single event upsets in neural networks operating for

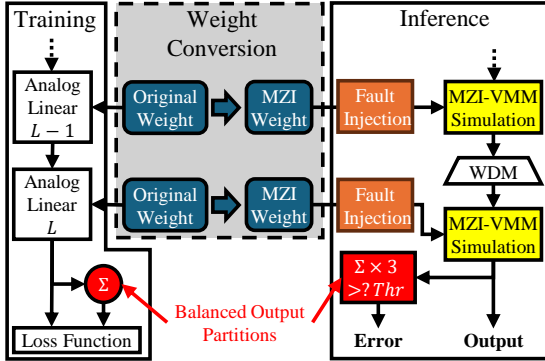


Fig. 4: The *SecONN* overview.

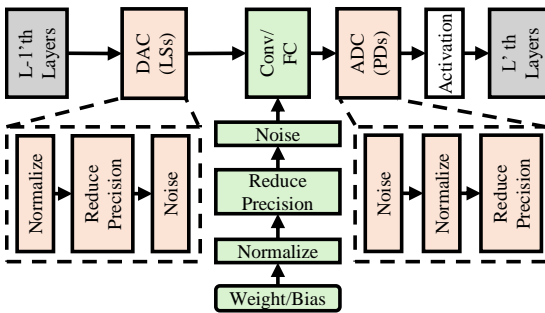
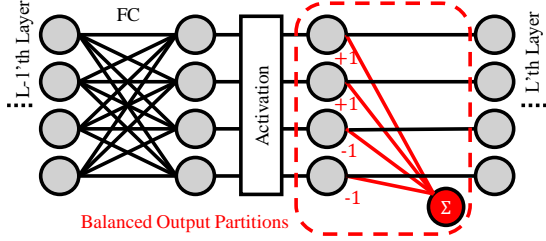
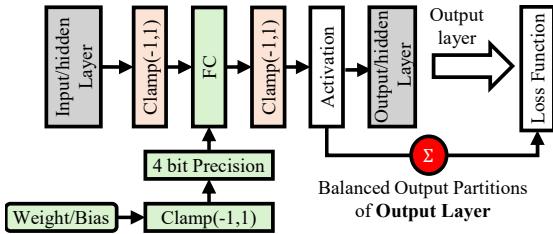


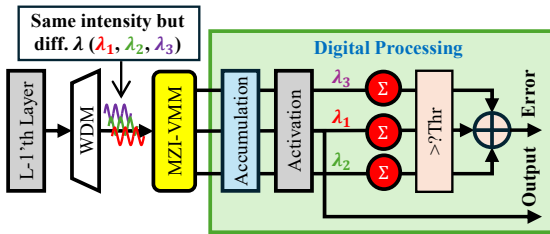
Fig. 5: An analog layer design.



(a) Balanced output partitions.



(b) Training architecture.



(c) Inference and runtime detection architecture (λ : Wavelength).

Fig. 7: *SecONN* training/inference architecture.

safety-critical digital systems. This paper proposes that this technique can be utilized for detecting thermal fault injection attacks on analog SPAAs. Balanced output partitions are designed to embed a balance checksum in deep neural networks. This paper adds an additional node with fixed weights in each layer as shown in Fig. 7a. The first half edges have a $+1$ weight value while the second half edges have a -1 weight value. If the checksum result exceeds a predetermined threshold, it is judged that the ONN is attacked. We assume the checksum for this additional node can be performed by a CMOS coprocessor. No additional hardware is required for optical circuits.

In this paper, we implement this method into the output layer as shown in Fig. 7b. Figure 7b shows the training architecture. We omit the “Reduce Precision” and the “Noise” layers in the original “DAC” and “ADC” layers to boost up the training speed in Fig. 5. Weights and biases are quantized with 4 bits. The detail of the inference phase is described in Sect. III-E.

E. WDP: Wavelength Division Perturbation

The balanced output partitions do not detect a fault injection attack if the attack does not impact on checksum results. For example, if the attack increases the sum of the first half and the sum of the second half of the output values in Fig. 7a by the same amount, the checksum result does not change, which leads to misdetection. To increase the detection capability, a

concept of *WDP* is proposed. The key point is ϕ s and θ s in Fig. 1c depend on the light wavelength. We input light signals with the same intensities but different wavelengths to ONNs. As a result, W in Eq. (1) is “perturbed” and transformed into a matrix with different element values. This changes the balance at the checksum node, thereby amplifying the effect of the abnormal phase shift even if the attack does not impact on checksum results with the original wavelength. *WDP* allows *SecONN* not only to perform inference in a target wavelength but also to detect attacks in all the wavelengths concurrently, which does not impact on the operating speed of the main inference operation. In order to separately get the checksum results, the number of checksum nodes in the output layer (“ Σ ” node in Fig. 7a) is set to be equal to the number of wavelengths.

Figure 7c shows a case where there are 3 wavelengths (λ_1 , λ_2 and λ_3) and three checksum nodes (“ Σ ”s) are used. The optical signal with λ_1 provides not only a VMM result but also a checksum result. The other two input signals with λ_2 , λ_3 have the same intensities as the original λ_1 signal. They are only concurrently used for obtaining checksum results. Since W elements differ by wavelengths, the three checksum results are different, thereby increasing the detectability. If at least one of the checksum results exceeds a predetermined threshold, it is judged that the ONN is attacked. The threshold is set to a positive number to reduce the misdetection (false negative) rate. This is because the checksum nodes alert for every inference operation if the threshold is too low (e.g., 0). The following features are implemented into the proposed simulator in order to incorporate the *WDP* effect:

Feature1: Phase shifters are the only wavelength-dependent elements. This can be achieved assuming that all the elements are symmetrically placed and that broadband couplers such as [25] are utilized for MZIs.

Feature2: Process variation impacts are negligible.

Feature3: Phase shifters have wavelength dependency. The dependency is defined as $\theta(\lambda) = \eta(\lambda)\theta_{\text{set}}$, where λ , θ , θ_{set} denote the wavelength, the actual amount of the phase shift and the phase shift we set, respectively. $\eta(\lambda)$ is 1 when the wavelength is 1550 nm. Detailed parameters of $\eta(\lambda)$ are based on actual silicon photonics chip parameters. Roughly speaking, $\eta(\lambda)$ is a function which is proportional to λ^{-1} .

Note that the key point is W in Eq. (1) depends on wavelength. We thus only limit the wavelength-dependent elements to phase shifters in this paper for simplicity.

IV. RESULTS AND DISCUSSION

A. Setup

We apply the proposed method to MNIST handwritten digit dataset classification [9]. A handwritten number of 28×28 pixels is reshaped to an array of 784×1 and is then input into the network. The neural network has three FCs with LeakyReLU as an activation function. The number of layers (L) is 3. The FCs transform the feature dimensions from 784 to 256, from 256 to 128, and from 128 to 10, respectively. The training dataset is split into training sets of 55000 examples and validation sets of 5000 examples by the stratified sampling.

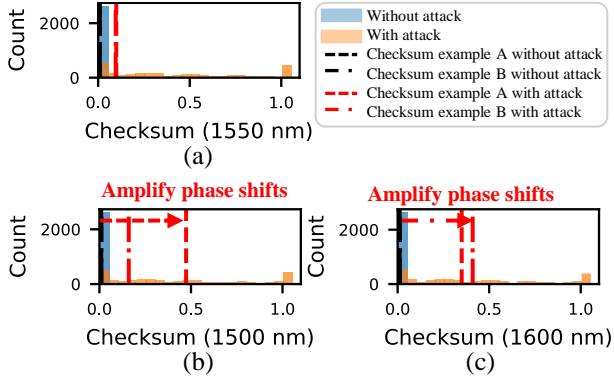


Fig. 8: The checksum distributions of attack-caused misprediction samples. (a) 1550 nm, (b) 1500 nm and (c) 1600 nm.

The training epoch is 50. The recognition accuracy achieves 97.8% with the simulation. Since the recognition accuracy of the model without balanced output partitions is 97.7%, the proposed concurrent detection does not degrade the model quality. The threshold is determined so that the misdetection (false negative) rate is 5% without attacks. The device setup is shown in TABLE I. This simulation adds the Gaussian noise with 0.02 standard deviation to the signals. This simulation also quantizes 4-bit in laser sources and homodyne detection. MZI-VMM can perform 16×16 sized matrix and the weight signals quantized 4 bit. We use 1550 ± 50 nm in WDP (i.e., $\lambda_1 = 1550$ nm, $\lambda_2 = 1500$ nm, $\lambda_3 = 1600$ nm in Fig. 7c). We assume one phase shifter in an SPAA is attacked during the inference operation of every sample. Phase shifts of $\pi/2$, π and $3\pi/2$ radian are injected to every phase shifter. For each injection, the checksums and the detection accuracy are evaluated with test datasets containing 10000 samples.

B. WDP Result

Figure 8 shows the checksum distributions using WDP. Figure 8 only counts attack-caused misprediction samples. The checksum results over 1.1 are omitted. Without attacks, the checksum results are located near “0.0”. On the other hand, if the attackers inject faults, the checksum results move to the right-hand side. This means that fault injection attacks can be concurrently detected while performing inference of input data. The black broken and the dash-dotted lines in Fig. 8 correspond to checksum examples A and B of single-fault injection, respectively. We do not see the significant unbalanced activities in the checksum results of example A for $\lambda_1 = 1550$ nm. However,

TABLE I: MZI-VMM parameters.

Settings		Parameters
Laser Sources	Reduce Precision	4 bit
	Noise deviation	0.02
Homodyne Detectors	Reduce Precision	4 bit
	Noise deviation	0.02
MZI-VMM Simulator	Block Matrix Size	16×16 ($N = 16$)
	Reduce Precision	4 bit
	Wavelengths	1550 ± 50

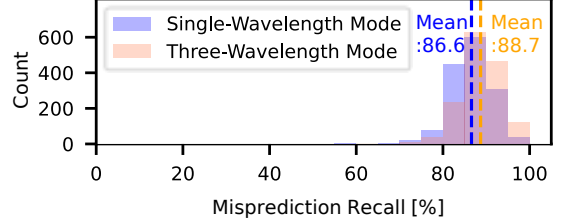


Fig. 9: The misprediction recall in each layer.

the $\lambda_2 = 1500$ nm and the $\lambda_3 = 1600$ nm checksum results amplify the effect of the attack. Similarly, the $\lambda_3 = 1600$ nm checksum result of example B amplifies the effect of the attack. This indicates that WDP boosts up the capability of concurrent detection of thermal fault injection attacks.

C. Detection Result

This paper then evaluates the attacks-caused misprediction recall.

A recall is defined as $Recall = TP / (TP + FN)$, where TP and FN denote the numbers of true positive and false negative samples, respectively.

Figure 9 shows the simulation result for the misprediction recall. In the single-wavelength mode, the average recall is 86.6%, and the minimum recall is 59.7%. Compared with the single-wavelength mode, the recall results improve in the multi-wavelength mode. The average recall is 88.7%, and the minimum recall is 60.3%. This shows that WDP is effective in amplifying the abnormal phase shifts while simultaneously performing inference of input data.

D. Latency Comparison

The MZI-VMM can perform $N \times N$ VMM in a single operation. The numbers of nodes in the input layer and all the three layers of the target DNN are 784, 256, 128 and 10, respectively. Since each layer has a bias node, the latency of a single sample inference is $(\lceil 785/N \rceil \cdot \lceil 256/N \rceil + \lceil 257/N \rceil \cdot \lceil 128/N \rceil + \lceil 129/N \rceil \cdot \lceil 10/N \rceil) D_0$ ($:= D_{SecONN}(N)$), where D_0 is the latency of the MZI-VMM.

The prior art [10] feeds the test signals into the ONNs and compares them with the expected outputs. There are two possible testing scenarios:

1) *Scenario 1*: Predetermined test images are fed into ONNs and a CMOS coprocessor checks whether they are correctly categorized by ONNs. In this case, at least 10 test images have to be fed into ONNs for the MNIST dataset with 10 categories. Since the MZI-VMM has the wavelength dependency, only a single wavelength can be used for obtaining accurate calculation results. If we put these test images into every input image, MZI-VMM has to categorize 11 images (10 predetermined test images and 1 input image). The latency becomes $11D_{SecONN}(N)$, which drastically degrades the inference latency compared with $SecONN$.

2) *Scenario2*: Predetermined test vectors are fed into MZI-VMM, and their outputs are examined in order to detect fault injection attacks by checking matrix elements. Assuming that attackers inject errors for every input image, MZI-VMM is tested at least once for every input image. Since the rank of the matrix at least once for every input image. Since the rank of the matrix expressed by the MZI-VMM is N , at least N test vectors are required to detect the attack by fully checking the matrix elements. Therefore, the latency of this scenario is $ND_0 + D_{\text{SecONN}}(N)$. If we put $N = 16$, this value corresponds to +1.7% latency overhead. The overhead superlinearly increases as N increases. The matrix size N of commercial ONNs such as Lightmatter's Mars [3] is 64. If we put $N = 64$, the overhead becomes +98%. This shows that the proposed technique is suitable for large-scaled ONNs.

V. CONCLUSION

This paper proposed *SecONN*, an optical neural network framework enabling not only inference operations but also concurrent detection of thermal fault injection attacks. This paper firstly shows the threat of thermal fault injection attacks using actual measurements. This indicates that attackers can tamper with the entire matrix elements in VMM. To tackle this issue, *SecONN* features concurrent detection of thermal fault injection attacks as well as simulation environment considering thermal fault injection attacks.

This paper then proposed *WDP* which fully exploits the nature of lights. This technique boosts the detection rate without degrading the operating speed. The evaluation results show that the proposed method achieves 88.7% attacks-caused average misprediction recall.

ACKNOWLEDGMENT

This work was supported in part by JSPS KAKENHI (Grant Number 23H04804), JST FOREST Program (Grant Number JPMJFR232Q, Japan), Research support program for JST-FOREST promoted by UOsaka. The authors thank Dr. Ryosuke Matsuo of Osaka University for assistance with measurement of silicon photonics chips. The authors thank Prof. Michihiro Shintani of Kyoto Institute of Technology and Prof. Masanori Hashimoto of Kyoto University for valuable advices on this research.

REFERENCES

- [1] "International Roadmap of Devices and Systems (IRDS). More Moore. 2023." Available online: <https://irds.ieee.org/editions/2023/20-roadmap-2023-edition/130-irds%E2%84%A2-2023-more-moore> (Accessed on Sep. 18, 2024.).
- [2] X. Wu, J. Xu, Y. Ye, Z. Wang, M. Nikdast, and X. Wang, "SUOR: Sectioned Unidirectional Optical Ring for Chip Multiprocessor," *J. Emerg. Technol. Comput. Syst.*, vol. 10, no. 4, Jun 2014. [Online]. Available: <https://doi.org/10.1145/2600072>
- [3] C. Ramey, "Silicon Photonics for Artificial Intelligence Acceleration : HotChips 32," in *2020 IEEE Hot Chips 32 Symposium (HCS)*, 2020, pp. 1–26.
- [4] K.-i. Kitayama, M. Notomi, M. Naruse, K. Inoue, S. Kawakami, and A. Uchida, "Novel frontier of photonics for data processing—Photonic accelerator," *APL Photonics*, vol. 4, no. 9, p. 090901, 09 2019.
- [5] Y. Liu, L. Wei, B. Luo, and Q. Xu, "Fault injection attack on deep neural network," in *2017 IEEE/ACM International Conference on Computer-Aided Design (ICCAD)*, 2017, pp. 131–138.
- [6] Y. Shen, N. C. Harris, S. Skirlo, M. Prabhu, T. Baehr-Jones, M. Hochberg, X. Sun, S. Zhao, H. Larochelle, D. Englund, and M. Soljačić, "Deep learning with coherent nanophotonic circuits," *Nature Photonics*, vol. 11, no. 7, pp. 441–446, Jul 2017.
- [7] W. R. Clements, P. C. Humphreys, B. J. Metcalf, W. S. Kolthammer, and I. A. Walsmley, "Optimal design for universal multiport interferometers," *Optica*, vol. 3, p. 1460, 12 2016.
- [8] K. Sanchez, R. Desplats, F. Beaudoin, P. Perdu, S. Dudit, M. Vallet, and D. Lewis, "Dynamic thermal laser stimulation theory and applications," in *2006 IEEE International Reliability Physics Symposium Proceedings*, 2006, pp. 574–584.
- [9] Y. LeCun, C. Cortes, and C. Burges, "MNIST handwritten digit database," *ATT Labs [Online]*. Available: <http://yann.lecun.com/exdb/mnist>, vol. 2, 2010.
- [10] F. G. De Magalhaes, M. Nikdast, and G. Nicolescu, "Integrated Photonic AI Accelerators Under Hardware Security Attacks: Impacts and Countermeasures," in *2023 IEEE 66th International Midwest Symposium on Circuits and Systems (MWSCAS)*, 2023, pp. 806–810.
- [11] D. Boneh, R. A. DeMillo, and R. J. Lipton, "On the importance of checking cryptographic protocols for faults," in *Advances in Cryptology — EUROCRYPT '97*, W. Fumy, Ed. Berlin, Heidelberg: Springer Berlin Heidelberg, 1997, pp. 37–51.
- [12] T. Fukunaga and J. Takahashi, "Practical fault attack on a cryptographic lsi with iso/iec 18033-3 block ciphers," in *2009 Workshop on Fault Diagnosis and Tolerance in Cryptography (FDTC)*, 2009, pp. 84–92.
- [13] S. Guillely, L. Sauvage, J.-L. Danger, N. Selmane, and R. Pacalet, "Silicon-level solutions to counteract passive and active attacks," in *2008 5th Workshop on Fault Diagnosis and Tolerance in Cryptography*, 2008, pp. 3–17.
- [14] S. P. Skorobogatov and R. J. Anderson, "Optical fault induction attacks," in *Cryptographic Hardware and Embedded Systems - CHES 2002*, B. S. Kaliski, ç. K. Koç, and C. Paar, Eds. Berlin, Heidelberg: Springer Berlin Heidelberg, 2003, pp. 2–12.
- [15] J. Breier, X. Hou, D. Jap, L. Ma, S. Bhasin, and Y. Liu, "Practical Fault Attack on Deep Neural Networks," in *Proceedings of the 2018 ACM SIGSAC Conference on Computer and Communications Security*, ser. CCS '18. New York, NY, USA: Association for Computing Machinery, 2018, p. 2204–2206.
- [16] F. Su, C. Liu, and H.-G. Stratigopoulos, "Testability and Dependability of AI Hardware: Survey, Trends, Challenges, and Perspectives," *IEEE Design & Test*, vol. 40, no. 2, pp. 8–58, 2023.
- [17] L. Liu, Y. Guo, Y. Cheng, Y. Zhang, and J. Yang, "Generating Robust DNN With Resistance to Bit-Flip Based Adversarial Weight Attack," *IEEE Transactions on Computers*, vol. 72, no. 2, pp. 401–413, 2023.
- [18] K. Matsuda, T. Fujii, N. Shoji, T. Sugawara, K. Sakiyama, Y.-I. Hayashi, M. Nagata, and N. Miura, "A 286 f2/cell distributed bulk-current sensor and secure flush code eraser against laser fault injection attack on cryptographic processor," *IEEE Journal of Solid-State Circuits*, vol. 53, no. 11, pp. 3174–3182, 2018.
- [19] M. Naruse, H. Hori, K. Kobayashi, and M. Ohtsu, "Tamper resistance in optical excitation transfer based on optical near-field interactions," *Opt. Lett.*, vol. 32, no. 12, pp. 1761–1763, Jun 2007.
- [20] J. Shiomi, S. Kotsugi, B. Dong, H. Onodera, A. Shinya, and M. Notomi, "Tamper-Resistant Optical Logic Circuits Based on Integrated Nanophotonics," in *2021 58th ACM/IEEE Design Automation Conference (DAC)*, 2021, pp. 139–144.
- [21] S. Jiao, Z. Song, and S. Xiang, "Adversarial Attacks on an Optical Neural Network," *IEEE Journal of Selected Topics in Quantum Electronics*, vol. 29, no. 2: Optical Computing, pp. 1–6, 2023.
- [22] E. Ozen and A. Orailoglu, "Concurrent Monitoring of Operational Health in Neural Networks Through Balanced Output Partitions," in *2020 25th Asia and South Pacific Design Automation Conference (ASP-DAC)*, 2020, pp. 169–174.
- [23] V. Shah and N. Youngblood, "AnalogVNN: A fully modular framework for modeling and optimizing photonic neural networks," *APL Machine Learning*, vol. 1, 6 2023.
- [24] "MZI-VMM_sim," Sep. 2024, [Online; accessed 14. Sep. 2024]. [Online]. Available: https://github.com/kawa-satoshi/MZI-VMM_sim
- [25] X. Liu, Y. Zhao, Z. Sheng, and F. Gan, "Compact and Ultra-Broadband Silicon Photonic Adiabatic Directional Coupler Using Rib Waveguides," *IEEE Photonics Technology Letters*, vol. 36, pp. 637–640, 5 2024.